Volterra Behavioral Model for Wideband RF Amplifiers

Carlos Crespo-Cadenas, *Associate, IEEE,* Javier Reina-Tosina, *Associate, IEEE* and María J. Madero-Ayora

***Abstract*— This paper proposes a behavioral modeling approach for the description of nonlinearities in wideband wireless communication circuits with memory. The model is formally derived exploiting the dependence on frequency of the amplifier nonlinear transfer functions and reduce the number of parameters in a general Volterra-based behavioral model. To validate the proposed approach, a commercial amplifier at 915 MHz, exhibiting nonlinear memory effects, has been widely characterized using different stimuli, including two tones, QPSK-WCDMA, and 16-QAM signals with rectangular and root-raised cosine conforming pulses. The theoretical results have been compared with experimental data demonstrating that the model performance is comparable to the well-established memory polynomial model. Calculated and measured baseband waveforms, signal constellation, spectral regrowth and ACPR are tightly coincident in all cases, emphasizing the relevance of the proposed model.**

***Index Terms*— Behavioral models, microwave amplifiers, Volterra series, nonlinear memory effects.**

I. Introduction

As a fundamental block in wireless communications systems, the power amplifier (PA) has undergone exhaustive study of its characteristics, in particular those related with nonlinear memory effects. Many efforts have been devoted to obtain behavioral models for microwave PAs, for which the output of this black-box method is predicted without knowledge of the nonlinear device internal structure. The goals of these approaches are, on the one hand, reduction of complexity maintaining an accuracy comparable to the results obtained with circuit-level simulations and, on the other hand, a simple method to extract the model parameters. An indicator of the importance of these approaches is the valuable work presented in the last years, for example [1]-[3], and the recent publication of an extensive revision related to this topic [4].

Exploiting the bandlimited character of wireless signals, PA description can be translated into an envelope representation and frequently has been deduced as Volterra series, a procedure that treats this problem in an strictly and orderly way. However, one difficulty of amplifier modeling using this Volterra approach is its high computational complexity [5]. The great number of coefficients required for the description of systems with a strong nonlinearity and long memory has steered the work of many researchers in order to reduce the number of model parameters. Probably, the most manageable solution to reduce the number of coefficients is the memory polynomial model proposed in [1], the structure of which presents a notable truncation in the number of parameters. Although the reduction obtained with this simplified Volterra model is important, the number of coefficients remains high, particularly in the case of amplifiers with long memory. To achieve a further reduction, an extension of the memory polynomial model with sparse delay tap structure was proposed in [2].

It is not clear how the parameter reduction of these particular structures affects the attainable accuracy of the model owing to the possible importance of other underestimated terms. Specifically, the need for considering those neglected terms was the purpose of the novel structure reported in [3]. That new approach is based on the pruning of redundant kernels in the full Volterra series model so that the coefficients with less effect on the output signal are discarded following an *a posteriori* procedure. Despite the significance of the cited models, it is desirable to develop an approach with an optimized number of coefficients, sustained on theoretical principles and with no need of a previous empirical selection. That was the aim of the author's initial study of an amplifier with one FET based on its simplified equivalent circuit. A third-order model was validated with experimental data and partial results were presented in [6].

In this paper the authors introduce the demonstration of a fifth order Volterra model for a general amplifier with bandwidth larger than the RF signal band. The approach allows the analysis of nonlinear memory effects from a model based on the transfer functions with no restrictions in the number or kind of nonlinear devices composing the amplifier. In the next section the study of a wideband amplifier and the completion of its behavioral model based on a Volterra series approach is described. The frequency independence of the amplifier response inside the RF bandwidth is exploited to reduce the order model and to reveal the dependence of coefficients extraction on the sampling rate. Section III is dedicated to describe the procedure of parameter extraction, which has been simplified because of order reduction in the model structure. Application of the method to a commercial amplifier and comparison with the memory polynomial model, and also with experimental data using different types of input signals, is presented to validate the demonstrated theoretical results. Finally, a generalization of the model to any order is proposed and some relevant statements are commented.

This work was completed with the support of the Spanish National Board of Scientific and Technological Research (CICYT) within the project TEC2004-06451-C05-03.

The authors are with the Departamento de Teoría de la Señal y Comunicaciones, Escuela Superior de Ingenieros, Universidad de Sevilla, Spain. E-mail: ccrespo@us.es, jreina@us.es, mjmadero@us.es

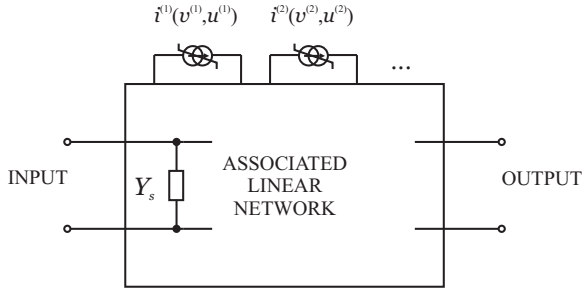

Fig. 1. General schematic of a nonlinear circuit.

II. Volterra Model for a Wideband Amplifier

A. Volterra-based behavioral model background

Let a general amplifier be represented by the circuit shown in Fig. 1. Nonlinearities are constituted by their linear components, included in the associated linear circuit, and nonlinear sources which are assumed to be dependent on two control voltages $v^{(a)}$ and $u^{(a)}$. Let the input $\tilde{x}(t)$ be an RF current excitation and $\tilde{y}(t)$ the output voltage corresponding to the fundamental frequency zone, centered at ω_c. Making use of the fact that a wireless signal commonly has a bandwidth B negligible with respect to the carrier frequency f_c, the discrete time-domain complex envelope Volterra model for this general nonlinear system can be expressed as

$$\begin{aligned} y(k) = &\sum_{q_1} h_1(q_1)x(k-q_1)+ \\ &+\sum_{\mathbf{q}_3} h_3(\mathbf{q}_3)x(k-q_1)x(k-q_2)x^*(k-q_3)+ \\ &+\sum_{\mathbf{q}_5} h_5(\mathbf{q}_5)x(k-q_1)x(k-q_2)x(k-q_3)\times \\ &\times x^*(k-q_4)x^*(k-q_5)+\cdots \end{aligned} \quad (1)$$

where $x(k)$ and $y(k)$ are complex envelope samples of the input and output RF signals, respectively, $h_n(\mathbf{q}_n)$ represents the discrete Volterra kernels of order n and $\mathbf{q}_n$ is an n-dimensional vector composed of the integer-valued delays q_i $(i=1,\cdots,n)$ [3]. Although a sampling rate equal to the input signal RF bandwidth is sufficient for memoryless nonlinear system identification [7], it should be increased according to the broadening of the output bandwidth B_o if aliasing has to be avoided. As a consequence, for an adequate representation of the output $y(t)$, the sampling time has to be reduced correspondingly to $t_s = 1/B_o$.

Equation (1) is a discrete-time Volterra series derived from the representation using the multidimensional nonlinear transfer functions (NLTF) $\tilde{H}_n(\boldsymbol{\omega})$ [8]. In continuous-time form, the n-th order term of the output signal can be written as

$$\begin{aligned} y_n(t) = \frac{2}{(4\pi)^n}\binom{n}{m}\int_{-\infty}^{\infty}\tilde{H}_n(\boldsymbol{\omega}_{cn}+\boldsymbol{\omega})\prod_{i=1}^{m+1}X(\omega_i)\times \\ \times\prod_{i=m+2}^{n}X^*(\omega_i)\exp(j\boldsymbol{\omega}'\mathbf{t})d\boldsymbol{\omega}, \end{aligned} \quad (2)$$

for $n=2m+1$. In (2), $\boldsymbol{\omega}_{cn}$ is a vector with its first $m+1$ components equal to ω_c and the remaining m components are equal to $-\omega_c$, $\boldsymbol{\omega}=(\omega_1,\cdots,\omega_n)'$ is a column vector having n baseband frequency components, $\boldsymbol{\omega}'$ is the transpose of $\boldsymbol{\omega}$ and $\mathbf{t}$ is a column vector with its n components equal to t.

The bandlimited condition of the input signal allows to neglect the integral outside two n-dimensional boxes with length B_o and centered at $\pm\boldsymbol{\omega}_{cn}$. Consequently, it is possible to substitute $\tilde{H}_n(\boldsymbol{\xi})$ with an equivalent transfer function bandlimited into these n-dimensional hypercubes, $\hat{H}_n(\boldsymbol{\xi})$, from which the bandlimited equivalent Volterra kernels are obtained making use of a multidimensional inverse Fourier transform. This equivalent transfer function and the discrete-time corresponding kernel $\hat{h}_n(\mathbf{q}_n)$ satisfy the relation

$$\hat{H}_n(\boldsymbol{\omega}_n) = \sum_{\mathbf{q}_n}\frac{\hat{h}_n(\mathbf{q}_n)}{B_o^n}\exp(-j\boldsymbol{\omega}_n'\mathbf{q}_n t_s). \quad (3)$$

Substitution in (2) allows to separate the integrals and to obtain the output component $y_n(t)$. Therefore, after sampling at instants $t=kt_s$, expression (1) is immediately derived.

The Volterra model (1) is a very general result but it has a high degree of difficulty due to the large number of parameters and numerical operations involved [5]. The complexity of the problem is revealed in the fact that the kernels $h_n(\mathbf{q}_n)$ form a n-dimensional grid defined by the discrete delays in each axis of the multidimensional space $q_1,\cdots,q_n$, hence it is desirable to reduce the number of these delays.

One of the most extended methods proposed to achieve a more manageable number of parameters is the memory polynomial model described in [1]. For this model the reduction in the number of coefficients is obtained by selecting only the delays positioned in the diagonal, i.e. the delays along the direction defined by $q_1=q_2=\cdots=q_n$. Moreover, if a sparse delay tap structure is adopted and only the most significant delays are retained following an *a posteriori* procedure, a further important cutback in the number of coefficients can be procured [2]. However, the model precision can be diminished due to the possible importance of non-diagonal terms. Following a more relaxed pruning approach, which also retains the terms near the diagonal, a more recent model was proposed with a consequent improvement in precision at the expense of a moderate increase in the number of coefficients [3].

Although the memory polynomial model has proven to be effective and the reduction of coefficients is considerable, the lack of a theoretical justification originates the need of these empirical-based methods. Additionally, important issues as the adequate sampling rate or the dependence of the discrete kernels on this sampling rate in (1), should be addressed by a behavioral model.

B. Nonlinear Transfer Functions for a Wideband Amplifier

A formal reduction in the number of coefficients in (1) can be obtained under the only assumption of a wideband amplifier, i.e. an amplifier with a pass band larger than the RF signal bandwidth. This supposition does not introduce any important loss of generality since many wireless amplifiers presenting nonlinear memory effects, have frequency

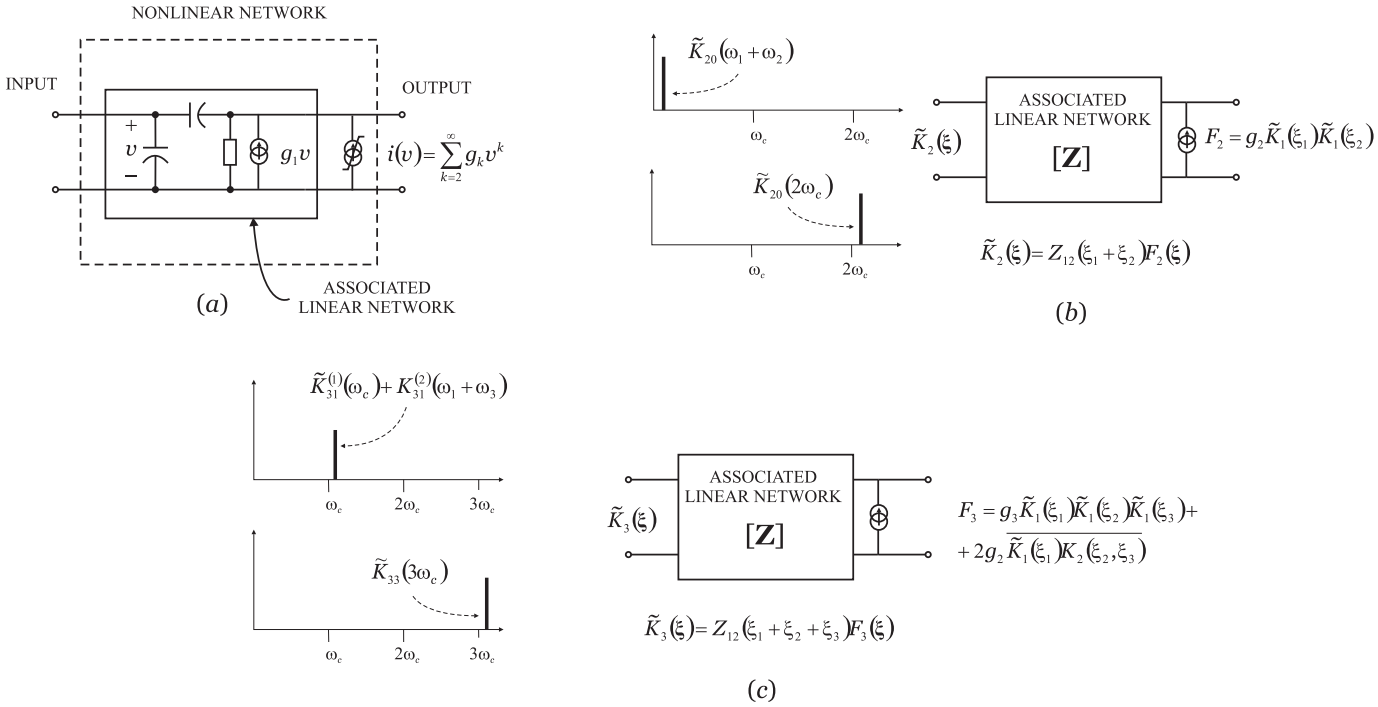

Fig. 2. Illustrative example to show frequency dependence of the nonlinear transfer functions. (a) Elementary nonlinear network. (b) Associated linear network excited by appropriate nonlinear currents and spectrum of the generated second-order transfer functions. (c) The same associated linear network producing the third-order transfer functions and their related spectrum.

responses essentially constant in their respective RF signal bands, see for example [2]. Under this assumption, completion of the particular frequency dependence of the transfer functions $\tilde{H}_n(\boldsymbol{\xi})$ for a typical circuit can be accomplished by a combination of the Probing Method and the Nonlinear Currents Method, a widespread procedure [10], [11].

For the general circuit of Fig. 1, the vector formed with the nonlinear transfer functions of order n relating the voltages of the independent ports of the associated linear network can be obtained by using the following equation

$$\tilde{\mathbf{H}}_n(\boldsymbol{\xi}) = -\mathbf{Y}^{-1}(\xi_1+\xi_2+\cdots+\xi_n)\tilde{\mathbf{F}}_n(\mathbf{i}_n) \qquad (4)$$

where $\mathbf{Y}(\xi)$ is the admittance matrix of the associated linear network and $\tilde{\mathbf{F}}_n(\mathbf{i}_n)$ is a vector with the spectral components of the nonlinear currents exciting the independent ports. The bandlimited condition of the wireless signal allows to extend the wideband amplifier assumption to all the harmonic zones so that the admittance matrix can be approximated by $\mathbf{Y}(l\omega_c+\omega) \approx \mathbf{Y}(l\omega_c)$ for $l=1,2,\cdots$, at all relevant values of ω. For an nth-order approximation the band of interest in the first harmonic zone should be here supposed to be nB.

For clarity, let consider only $\tilde{K}_n(\boldsymbol{\xi})$, the transfer functions relating the input with the voltage at the port of one nonlinearity, typically a voltage controlled current source, a conductance or a capacitance. To illustrate the procedure, an elementary circuit with a nonlinear current source is shown in Fig. 2 and a sketched summary of the method is attached. In the example, a nonlinear current source dependent on voltage v is considered as the main nonlinearity. For each order the associated linear network is excited by appropriate nonlinear currents in order to obtain the transfer functions relating voltage v with the input. Spectra show the prevalent components for orders 2 and 3.

The wideband condition of the amplifier allows to approximate the linear function $\tilde{K}_1(\omega_c)$ as a coefficient independent of baseband frequencies. The same is true for the transfer function relating the linear part of the output with the input, $\tilde{H}_1(\omega_c)$.

The spectral components function $\tilde{F}_2(\boldsymbol{\xi})$ can depend on the sum of baseband frequencies $\omega_i+\omega_j$, as is the case of a nonlinear capacitance, or is independent of baseband frequencies for other nonlinearities. In any case, since the components of the admittance matrix have this same dependence, the second-order nonlinear transfer function $\tilde{K}_{20}(\omega_i+\omega_j)$ depends on $\omega_i+\omega_j$ (with $\xi_i=\omega_c+\omega_i$ and $\xi_j=-\omega_c+\omega_j$) in the dc zone, and can be considered as a constant coefficient in the second-harmonic zone (see Table I). Notice that if other nonlinearities are present, their contribution is superposed at the same frequencies and therefore, the type of dependence remains unchanged.

Both in the fundamental frequency and in the third-harmonic zones, the admittance matrix is a function only of the carrier frequency, because the baseband frequency dependence of the third-order transfer function $\tilde{K}_3(\boldsymbol{\xi})$ is due to the spectral components of $\tilde{F}_3(\boldsymbol{\xi})$. Taking into account that this dependence comes from $\tilde{K}_2(\boldsymbol{\xi})$, in the fundamental frequency zone it is possible to determine two types of terms: a baseband frequency independent term $\tilde{K}_{31}^{(1)}$, and terms of the form $\tilde{K}_{31}^{(2)}(\omega_i+\omega_j)$. In the third-harmonic zone this transfer function does not present dependence on baseband frequencies. The type of dependence described above is in agreement with previously published results [12]-[16].

Although the extension of the analysis focused to the

TABLE I

TYPES OF BASEBAND FREQUENCY DEPENDENCE FOR $\tilde{K}_n(\boldsymbol{\xi})$

Frequency zone	$\tilde{K}_1(\xi)$	$\tilde{K}_3(\boldsymbol{\xi})$
1st. harmonic	$\tilde{K}_1$	$\tilde{K}_{31}^{(1)}$ $\tilde{K}_{31}^{(2)}(\omega_i+\omega_j)$
3rd. harmonic	–	$\tilde{K}_{33}$

Freq. zone	$\tilde{K}_2(\boldsymbol{\xi})$	$\tilde{K}_4(\boldsymbol{\xi})$
dc	$\tilde{K}_{20}(\omega_i+\omega_j)$	$\tilde{K}_{40}^{(1)}(\bar{\omega})$ $\tilde{K}_{40}^{(2)}=\alpha(\bar{\omega})\kappa_{40}^{(2)}(\omega_i+\omega_j)$ $\tilde{K}_{40}^{(3)}=\alpha(\bar{\omega})\kappa_{40}^{(3)}(\omega_i+\omega_j)\times$ $\times\kappa_{40}^{(3)}(\omega_{i'}+\omega_{j'})$
2nd. harmonic	$\tilde{K}_{22}$	$\tilde{K}_{42}^{(1)}$ $\tilde{K}_{42}^{(2)}(\omega_i+\omega_j)$
4th. harm.	–	$\tilde{K}_{44}$

The following definitions have been used: $\bar{\omega}=\omega_1+\omega_2+\omega_3+\omega_4$, $\xi_{i,i'}=\omega_c+\omega_{i,i'}$ and $\xi_{j,j'}=-\omega_c+\omega_{j,j'}$, $i\neq i'$ and $j\neq j'$.

TABLE II

TYPES OF BASEBAND FREQUENCY DEPENDENCE FOR $\tilde{H}_5(\boldsymbol{\xi})$

Type	$\tilde{H}_5(\xi)$
1	$\tilde{H}_{51}^{(1)}$
2	$\tilde{H}_{51}^{(2)}(\omega_i+\omega_j)$
3	$\tilde{H}_{51}^{(3)}=\eta_{51}^{(3)}(\omega_i+\omega_j)\eta_{51}^{(3)}(\omega_{i'}+\omega_{j'})$
4	$\tilde{H}_{51}^{(4)}(\omega_i+\omega_j+\omega_{i'}+\omega_{j'})$
5	$\tilde{H}_{51}^{(5)}=\alpha(\omega_1+\omega_2+\omega_3+\omega_4)\eta_{51}^{(5)}(\omega_i+\omega_j)$
6	$\tilde{H}_{51}^{(6)}=\alpha(\omega_1+\omega_2+\omega_3+\omega_4)\eta_{51}^{(6)}(\omega_i+\omega_j)\eta_{51}^{(6)}(\omega_{i'}+\omega_{j'})$

The generic functions η_{51} have the specific dependence on the sum of two baseband frequencies.

deduction of closed form expressions for higher order transfer functions is almost beyond the bounds of possibility, keeping track of their frequency dependence is a more feasible exercise. Next, this study is widened to higher order nonlinear transfer functions.

The cause of frequency dependence in $\tilde{K}_4(\boldsymbol{\xi})$ is twofold. On the one hand, the admittance matrix can be approximated by $\mathbf{Y}(\omega_1+\omega_2+\omega_3+\omega_4)$ in the dc zone, and by a frequency independent function in the second-harmonic and fourth-harmonic zones. On the other hand, the component $\tilde{F}_4(\boldsymbol{\xi})$ presents several terms with products of the transfer functions $\tilde{K}_1$, $\tilde{K}_2$ and $\tilde{K}_3$.

Summarizing, in the dc zone the fourth-order transfer function is composed by: one term that can be expressed by $\tilde{K}_{40}^{(1)}(\omega_1+\omega_2+\omega_3+\omega_4)$, a second type of terms $\tilde{K}_{40}^{(2)}=\alpha(\omega_1+\omega_2+\omega_3+\omega_4)\kappa_{40}^{(2)}(\omega_i+\omega_j)$, and a third type of terms with the form $\tilde{K}_{40}^{(3)}=\alpha(\omega_1+\omega_2+\omega_3+\omega_4)\kappa_{40}^{(3)}(\omega_i+\omega_j)\kappa_{40}^{(3)}(\omega_{i'}+\omega_{j'})$. It has been considered that $\xi_{i,i'}=\omega_c+\omega_{i,i'}$ and $\xi_{j,j'}=-\omega_c+\omega_{j,j'}$, for $i=1,2$ and $j=3,4$ with $i\neq i'$ and $j\neq j'$ (see Table I). Note that $\tilde{K}_{40}^{(2)}$ is represented as the product of two separated functions, α and $\kappa_{40}^{(2)}$, and in the same form, $\tilde{K}_{40}^{(3)}$ is denoted by the product of the functions α and $\kappa_{40}^{(3)}$. In these expressions, α is a generic function with the specific dependence on the sum of four baseband frequencies and $\kappa_{40}^{(2,3)}$ are generic functions dependent on the sum of two baseband frequencies. The significance of this particular frequency dependence is discussed below.

In the second-harmonic zone there are two type of terms, $\tilde{K}_{42}^{(1)}$ and $\tilde{K}_{42}^{(2)}(\omega_i+\omega_j)$, and in the fourth-harmonic zone there is only one (frequency independent) term, $\tilde{K}_{44}$. The explicit dependence has been omitted in the components that are only functions of the carrier frequency. These arguments are sufficient to deduce the frequency behavior of the relevant output transfer functions $\tilde{H}_3(\boldsymbol{\xi})$ and $\tilde{H}_5(\boldsymbol{\xi})$.

The transfer function $\tilde{H}_3(\boldsymbol{\xi})$ has a frequency dependence similar to $\tilde{K}_3(\boldsymbol{\xi})$, discussed above. In the case of $\tilde{H}_5(\boldsymbol{\xi})$, considering that the admittance matrix does not introduce any frequency dependence, its behavior is determined by $\tilde{F}_5(\boldsymbol{\xi})$, or equivalently, by the functions $\tilde{K}_1(\boldsymbol{\xi})$ to $\tilde{K}_4(\boldsymbol{\xi})$. Recalling that the zone of interest is the fundamental frequency zone, the relevant transfer functions can be represented by the 6 types of terms shown in Table II. Observe that now there are four different types of terms with a complete dependence on all the frequencies ω_1 to ω_4.

These results can be exploited to reduce the number of parameters in the behavioral model (1) without the addition of any other restriction.

C. Kernels of the reduced-order behavioral model.

1) Third order kernel: Based on the previous deductions, the third-order term of the output voltage is obtained by substituting in (2) the corresponding components $\tilde{H}_{31}^{(1)}$ and $\tilde{H}_{31}^{(2)}(\omega_1+\omega_2)$. The first type generates the memoryless term, and the second type gives rise to the generic expression

$$y_3^{(2)}(t)=\frac{3}{4(2\pi)^2}x(t)\int_{-\infty}^{\infty}\tilde{H}_{31}^{(2)}(\omega_1+\omega_2)\times \\ \times X(\omega_1)X^*(\omega_2)\exp(j\omega_1 t+j\omega_2 t)d\omega_1 d\omega_2. \quad (5)$$

Although this is a double integral, the transfer function is a one-dimensional function, a fact that can be explicitly displayed with a change to the new variables $\omega=\omega_1+\omega_2$ and $\xi=(\omega_2-\omega_1)/2$, for which $d\omega_1 d\omega_2=d\omega d\xi$, so that

$$y_3^{(2)}(t)=\frac{3}{4}\frac{1}{(2\pi)^2}x(t)\int_{-\infty}^{\infty}\tilde{H}_{31}^{(2)}(\omega)\times \\ \times X(\omega/2-\xi)X^*(\omega/2+\xi)\exp(j\omega t)d\omega d\xi. \quad (6)$$

Relying on the bandlimited assumption of $x(t)$, the integral in ω is negligible outside any bandwidth $B_o\geq 2B$, allowing the definition of an equivalent transfer function $\hat{H}_3(\omega)$ confined to this band. Making use of the Fourier transform and for frequencies inside B_o, $\hat{H}_3(\omega)$ can be expressed in terms of its discrete impulse response

$$\hat{H}_3(\omega)=\frac{1}{B_o}\sum_q \hat{h}_3(q)\exp(-jq\omega t_s), \quad (7)$$

so that the sampling time $t_s=1/B_o$ should be, at least, half the symbol period. Substituting in (6) and changing now to

the original variables, the two integrals become separable

$$y_3^{(2)}(t) = \frac{3}{4B_o}x(t)\sum_q \hat{h}_3(q)\frac{1}{(2\pi)^2}\times$$
$$\times \int_{-\infty}^{\infty} X(\omega_1)X^*(\omega_2)\exp[j\omega_1(t-qt_s)+j\omega_2(t-qt_s)]d\boldsymbol{\omega} =$$
$$= \frac{3}{4B_o}x(t)\sum_q \hat{h}_3(q)|x(t-qt_s)|^2. \quad (8)$$

Finally, after adding the memoryless part and sampling at instants $t = kt_s$, the third-order term of the output complex envelope can be expressed in a discrete-time form

$$y_3(k) = \sum_q h_3(q)|x(k-q)|^2x(k). \quad (9)$$

When the memoryless term is included in (9), we obtain the following expression for the third-order coefficients

$$h_3(q) = \begin{cases} \frac{3}{4}[\tilde{H}_{31}^{(1)} + \frac{1}{B_o}\hat{h}_3(0)], & \text{for } q = 0 \\ \frac{3}{4B_o}\hat{h}_3(q), & \text{for } q \neq 0. \end{cases} \quad (10)$$

2) Fifth order kernel: According to the previous discussion, the fifth-order transfer function is composed by 6 different types of terms which produce a particular set of kernels after substitution in (2). Like in the third-order transfer function, one of the five integrals involved gives rise again to $x(t)$, remaining in this case a quadruple integral, for which the first type of terms can be computed directly to contribute only to memoryless nonlinear effects. The second type of terms depends on $\omega_i+\omega_j$, so that only two integrals can be computed directly and the other two can be handled as in the third-order case producing one-dimensional kernels of the type

$$y_5^{(2)}(k) = \sum_q h_5^{(2)}(q)|x(k-q)|^2|x(k)|^2x(k). \quad (11)$$

For the other four types it is possible to write a generic fifth-order transfer function with a frequency dependence given by $\tilde{H}_5(\omega_1+\omega_3, \omega_2+\omega_4)$, where $\omega_{1,2}$ and $\omega_{3,4}$ are defined around ω_c and $-\omega_c$, respectively. Let consider the different properties of symmetry that this function can present, beginning with the more general condition corresponding to the fifth and sixth types of terms. At a first glance, the multiple integral in (2) is negligible outside a four-dimensional cube of length $4B$. However, the particular symmetry of $\tilde{H}_5$ involves a bidimensional frequency dependence that is exhibited clearly after the change of variables $\xi_1 = \omega_1 + \omega_3$, $\xi_2 = \omega_2 + \omega_4$, $\xi_3 = (\omega_3 - \omega_1)/2$ and $\xi_4 = (\omega_4 - \omega_2)/2$:

$$y_5^{(5)}(t) = \frac{5}{8}\frac{1}{(2\pi)^4}x(t)\int_{-\infty}^{\infty} d\xi_3 d\xi_4 \cdots$$
$$\cdots \int_{-\infty}^{\infty} \tilde{H}_5(\xi_1,\xi_2)X(\xi_1/2-\xi_3)X(\xi_2/2-\xi_4)\times$$
$$\times X^*(\xi_1/2+\xi_3)X^*(\xi_2/2+\xi_4)\exp(j\xi_1 t + j\xi_2 t)d\xi_1 d\xi_2. \quad (12)$$

Therefore, $\tilde{H}_5(\xi_1,\xi_2)$ is negligible outside any square of length $B_o \geq 2B$ and can be substituted by its equivalent function. It is possible to express this bandlimited function as a relation between the corresponding discrete-time kernels

$$\hat{H}_5^{(5)}(\boldsymbol{\xi}_2) = \frac{1}{B_o^2}\sum_{\mathbf{q}_2}\hat{h}_5^{(5)}(\mathbf{q}_2)\exp(-j\mathbf{q}_2'\boldsymbol{\xi}_2 t_s). \quad (13)$$

Substituting in (12) and changing to the original variables, the four integrals are now separable and, sampling at instants kt_s, the output in discrete-time form can be written as

$$y_5^{(5)}(k) = \sum_{q_1,q_2} h_5^{(5)}(q_1,q_2)|x(k-q_1)|^2|x(k-q_2)|^2x(k) \quad (14)$$

with

$$h_5^{(5)}(q_1,q_2) = \frac{5}{8B_o^2}\hat{h}_5^{(5)}(q_1,q_2). \quad (15)$$

It is immediate to note that $h_5^{(3)}$, related with the third type $\tilde{H}_{51}^{(3)}$, is a particular case of this result in which the transfer function is directly separable.

More revealing is the fourth type $\tilde{H}_{51}^{(4)}$, which involves the sum of all frequencies so that it presents the highest degree of symmetry and produces terms given by

$$y_5^{(4)}(k) = \sum_q h_5^{(4)}(q)|x(k-q)|^4x(k) \quad (16)$$

with

$$h_5^{(4)}(q) = \frac{5}{8B_o}\hat{h}_5^{(4)}(q). \quad (17)$$

Notice that for this particular coefficients, the sampling rate should be at least four times the symbol rate.

As a conclusion to this section, let observe that the demonstrated Volterra behavioral model incorporates a substantial reduction in the number of parameters, when compared to (1), with the only assumption of a wideband amplifier. Surprisingly, the described representation exhibits an exclusively "out of diagonal" structure, different to other well-known published behavioral models [1],[2].

To corroborate these new results, an amplifier has been tested and the model parameters have been extracted from experimental data, as discussed in the next section.

III. Model parameters extraction and validation

The commercial amplifier MAX2430 manufactured by MAXIM Integrated Products Inc. (Sunnyvale, CA), has been modeled with the present structure. It is a wideband amplifier at 915 MHz, however, in the experimental characterization with two tones separated 2 MHz, the amplifier exhibited an asymmetry in the IMD products, a clear indication of the existence of nonlinear memory effects. The measurement setup used in this study is basically the same as that presented in [15]. However, the excitations taken into account are diverse in order to test the proposed model with a wide variety of signals. In particular, standard two-tone as well as digitally modulated signals like QPSK-WCDMA, 16-QAM with rectangular pulses and root-raised cosine pulses have been used as input stimuli. These signals have been loaded in the internal memory of an SMIQ02B signal generator with built-in arbitrary waveform facility and the E4407B spectrum analyzer with a modulation analysis option has been used to acquire the baseband signal at the amplifier's output.

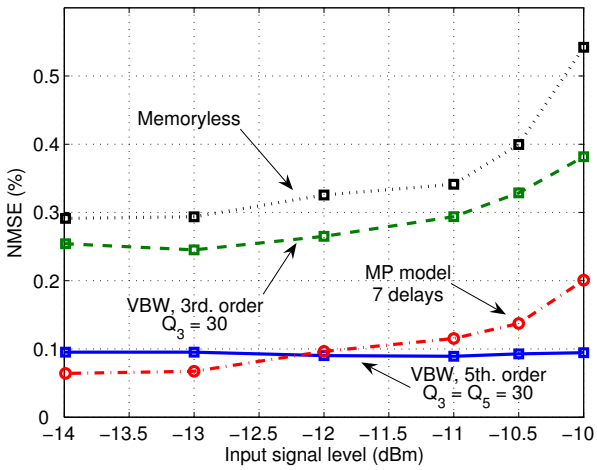

Fig. 3. Normalized error as a function of the input level. Proposed VBW model (squares and solid line) and memory polynomial (MP) model (circles and dot-dash line).

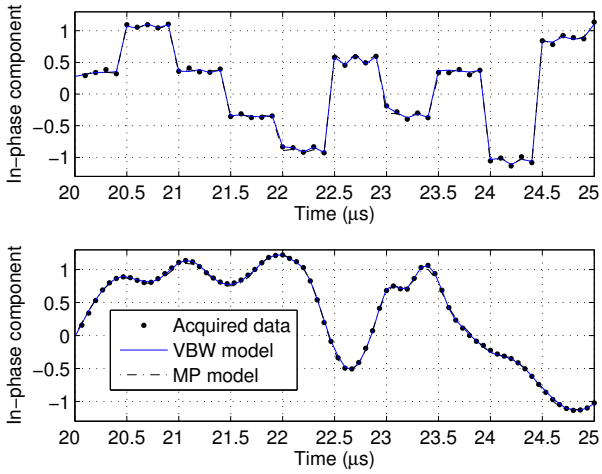

Fig. 4. Normalized complex envelope in-phase component for a 16-QAM signal. a) Rectangular pulses and b) Root-raised cosine pulses. Acquired data: dots. VBW model: solid line. MP model: dot-dash line.

A. *16-QAM signal with rectangular pulses*

As was demonstrated in the previous section, it is necessary to use a sampling rate of about four times the symbol rate if parameters up to the fifth-order have to be extracted. In the case of root-raised cosine modulating pulses, each sample is dependent on previous and future samples, included those many symbols away. Even in the case of a memoryless amplifier the output will display memory and it is therefore reasonable to use for nonlinear characterization modulating pulses without inter symbol interference, i.e. with length no longer than a symbol period. Consequently, the use of an RF signal modulated with rectangular pulses as an input stimulus guarantees that memory effects, if present in the output, have been caused by the nonlinear memory of the device. The modulation format is also relevant because it is well known that for PSK signals, a third-order model can capture some of the higher order nonlinear characteristics and produce degeneration in the parameter extraction process [9].

According to the above considerations, a 915 MHz carrier modulated with a random train of rectangular pulses at 2 Msymb/s and a 16-QAM format, was selected as the first sounding signal. The arbitrary waveform generator can handle up to 40 Msa/s so that the shape of the pulses was rather rectangular. Since in the recovery part the setup has a sampling rate of 15 Msa/s, the acquired output signals were sampled at 7.5 samples per symbol, amply suitable for signal representation and fifth-order parameters extraction. A fifth-order Volterra behavioral model for wideband amplifiers (VBW) was extracted from the acquired output complex envelope samples through the minimization of the average normalized mean square error (NMSE) between measured and modeled outputs. A first result is shown in Fig. 3, where the normalized error is plotted as a function of the input level. The error is represented in dotted line for a memoryless model and the dashed line corresponds to the results for a third-order VBW model with a memory of $Q_3 = 30$ samples. In both cases the error grows up as the amplifier enters in a more nonlinear condition indicating

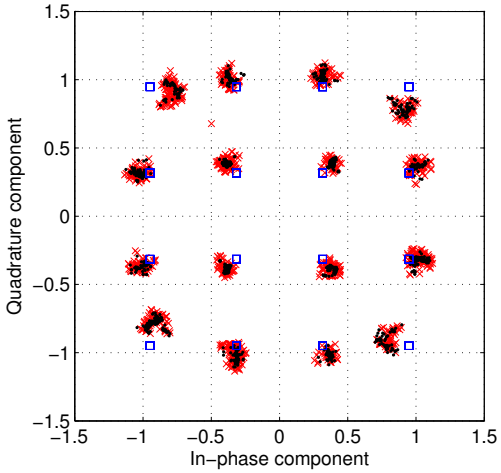

Fig. 5. Vector representation of the 16-QAM signal with rectangular pulses. Input signal: squares. Acquired data: crosses. VBW model: dots.

in the first case the presence of nonlinear memory and, in the second case, that not all the nonlinear memory coefficients have been extracted. On the contrary, the fifth-order VBW model depicted in solid line shows a very low error, constant in all the range of input levels, which is an evident confirmation of a correct parameters identification of the memory nonlinear model. To corroborate the validity of the present results, the well-established memory polynomial model (MP) described in [2] was extracted with a generous number of delays, and taken as a reliable reference. The error for this model with seven delays is represented in the same figure (dash-dot line) demonstrating a similar performance with respect to the VBW model. Furthermore, in the range of higher levels, the most relevant to this context, the VBW model outperforms the MP model.

The corresponding time-domain in-phase component for an input level of -11 dBm is shown normalized in Fig. 4a). The acquisitions (dots), the prediction of the MP model (dash-dot

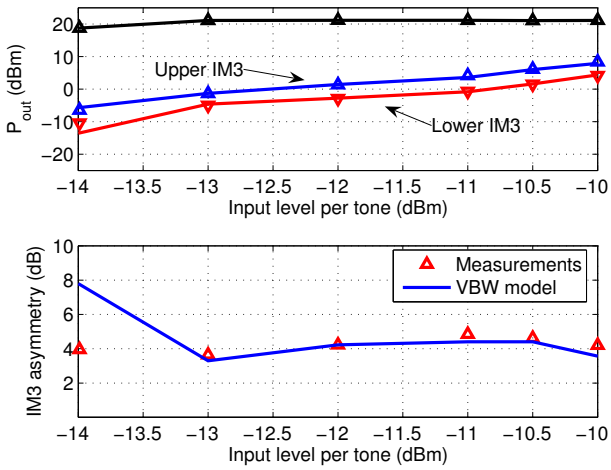

Fig. 6. Measured and simulated results for IM3 when tone spacing is 2 MHz. Acquired data: triangles. VBW model: solid line.

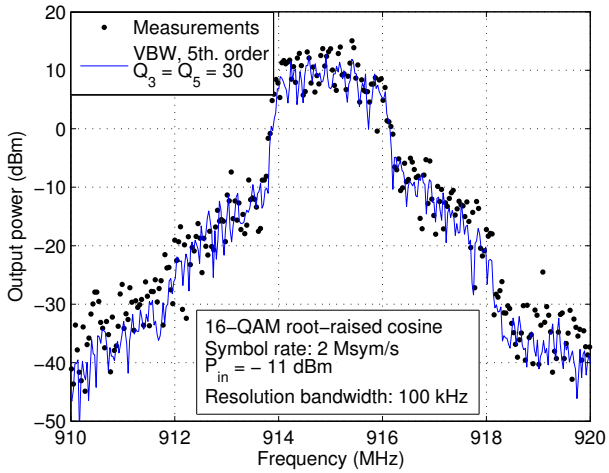

Fig. 7. Output spectrum of a 16-QAM signal with 2 Msymb./s. Root-raised conforming pulses. $P_{in} = -11$ dBm. Spectrum analyzer trace (dots) and VBW model prediction (solid line).

line) and the prediction of the present VBW model (solid line) have been represented. The average NMSE of the VBW model is -30.5 dB, representing 1 dB of improvement compared to the MP model. The vector representation of the modeled complex envelope is plotted with dots in Fig. 5 and compared with the input envelope (squares) and the acquired output (crosses).

B. Two tone signal

Another set of experiments was performed using an input signal formed by two tones of equal magnitude and phase, with a frequency separation of 2 MHz, and measuring the upper and lower third-order IM products. When the amplifier is working in linear mode the IM products are negligible compared to the non-systematic errors of the measurement setup, so that model parameters extracted from acquisitions at low signal levels are irregular. This is not specially inconvenient, because the interest is in the range of high signal levels, where the nonlinear effects are more relevant and model parameters can be reliably extracted. For that reason, after rejection of meaningless data, the experimental points represented in Fig. 6 belong to levels near the 1 dB compression point. In Fig. 6a) the measured output of the fundamental tones and the third-order intermodulation products (IM3) are represented with marks. In the same figure the results of the extracted model are depicted in solid line, reflecting a remarkable correspondence with the acquired data. According to the previous discussion, the difference between measured and calculated lower IM3 at -14 dBm is caused by setup limitation at low input levels. On the contrary, the significant coincidence inside the faithful range is also revealed when measured and predicted asymmetries are compared, as it is shown in Fig. 6b).

C. 16-QAM signal with root-raised cosine pulses

Another type of sounding signal employed in the extraction process has been a carrier at 915 MHz modulated in a 16-QAM format with a 2 Msymb/s train of symbols using root-raised cosine pulses. The acquired normalized in-phase component and the corresponding waveform obtained

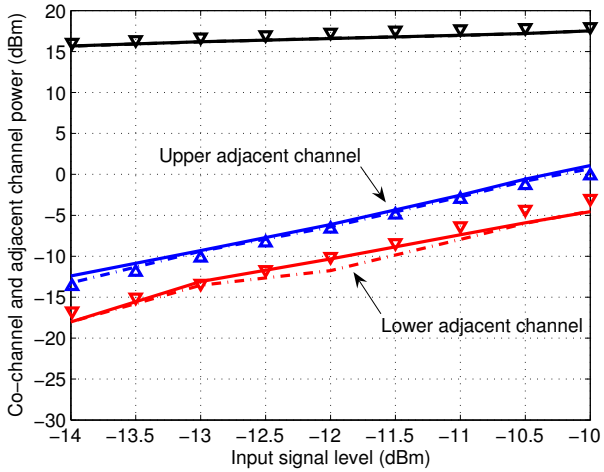

Fig. 8. In-channel and adjacent channel power. Acquired data: triangles. VBW model: solid lines. MP model: dot-dash lines

with the extracted model are represented in Fig. 4b) (dots and solid line, respectively). For comparison purposes, the waveform obtained with the memory polynomial model is also depicted in the same figure (dash-dot line). As a further test, the extracted model was used to predict the spectrum of the signal and the adjacent-channel power (ACP) in order to be compared with other alternative measurements using the conventional spectrum analyzer without the acquisition facility. The results are plotted in Figs. 7 and 8 using marks for the experimental data and solid lines for the modeled output. It is worth to note that the model was first extracted from an experimental acquisition of baseband samples and served to predict the output signal spectrum. Although the marks represent a measurement process independent of the acquisition, the prediction is favorably compared in Fig. 7. The second figure corroborates this outcome showing a good match between the adjacent channel power measured and calculated. The prediction is also able to estimate adequately

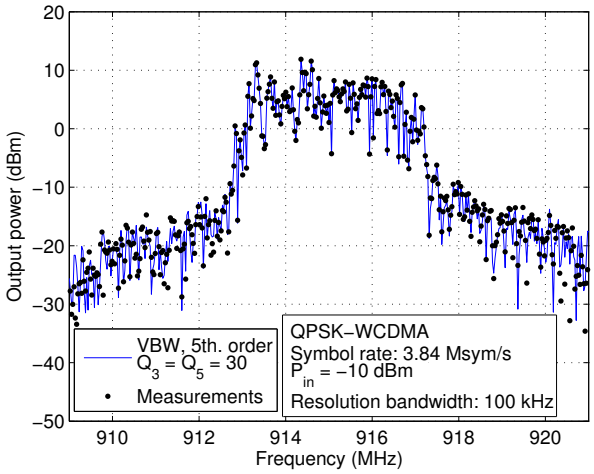

Fig. 9. Spectral regrowth of a W-CDMA signal with 3.84 Msymb./s. $P_{in} = -10$ dBm. Spectra of acquired data (dots) and model output (solid line).

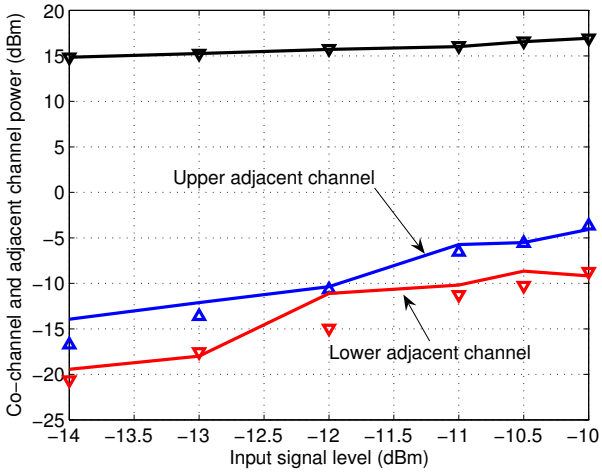

Fig. 10. ACP measured and calculated with the proposed method. Acquired data: triangles. VBW model: solid lines.

the ACP asymmetry between upper and lower channels. As a reference, the dash-dot line represents the results of the memory polynomial model.

D. QPSK-WCDMA signal

Finally, a carrier at 915 MHz modulated with a WCDMA signal compliant with the UMTS standard was employed as input signal. In this case, the condition of four times the symbol rate to correctly identify fifth-order parameters, 4×3.84 Msymb/s, just exceeds the sampling rate, 15 Msa/s.[1] However, the model has been able to extract adequately the parameters, as can be verified by comparing the acquired and modeled spectra, which are shown in Fig. 9 with dots for the experimental data and solid line for the calculations with the extracted model. Again, the present approach allows

[1]Considering that with respect to the modulation format the term *chip* ultimately corresponds to a symbol, in this context we use the term *symbol* instead of *chip*.

TABLE III
ACPR FOR A QPSK-WCDMA SIGNAL AT 3.84 MSPS.

$P_{in} = -10$ dBm.

Channel	Measured (dBc)	MP model (dBc)	VBW model (dBc)
Upper	-21.6	-20.4	-21.0
Lower	-24.7	-25.2	-26.1

a reliable prediction of ACP and its asymmetry from the acquired spectra, as can be confirmed in Fig. 10, in which the measured data (triangles) and the model results (solid lines) are represented.

An alternative method was used to measure the ACP with an input level of -10 dBm and the measured data are presented in Table III for the two adjacent channels. In the same table the calculations with the proposed VBW model are shown. In spite of the fact that the acquisitions were accomplished beyond the limits of the theoretical accuracy, a satisfactory agreement is revealed. For sake of comparison, the reference MP model is also included, attaining equivalent results.

IV. FINAL DISCUSSION AND CONCLUSIONS

This work demonstrates a new Volterra approach to model wideband amplifiers with nonlinear memory. The main characteristic of the present behavioral model is that it has been formally derived starting from a conventional nonlinear circuit analysis and makes possible to propose the extension of its structure to give the following equation

$$y(k) = h_1 x(k) + \sum_{m=1}^{\infty} \sum_{\mathbf{q}_m} h_{2m+1}(\mathbf{q}_m) \prod_{p=1}^{m} |x(k-q_p)|^2 x(k). \tag{18}$$

This expression has a remarkable difference with respect to the memory polynomial model consisting in the absence of the so-called "diagonal terms". Although only the assumption of a frequency independent response has been necessary to obtain the new model, the huge number of coefficients associated to the general discrete-time Volterra series has been drastically reduced. The parameter order reduction can be quantified for an example in which a fifth-order model with $Q = 3$ delays is considered. Taking into account symmetry considerations, 244 coefficients are necessary with the general Volterra model. As a reference, recall that in the MP model a total of 12 diagonal coefficients are needed, and a total of 54 or 133 coefficients form the model with the "near-diagonality" structural restriction $l = 1$ or $l = 2$, respectively [3]. Instead, the present model would need 21 coefficients. It is worth to observe that a fair comparison between the previous models and the present VBW would be only possible if some procedure of pruning to optimize the number of coefficients were also included.

In relation to memoryless nonlinear systems, the introduced analysis states that identification may be achieved by sampling at the symbol rate, in accordance with previously published results [17]. However, it is also demonstrated that in the case of systems with nonlinear memory, an increase of $n-1$ in the sampling rate is necessary to adequately identify nth-order parameters.

Another notable conceptual issue is the exhibited relation of the model coefficients, $h_n(\mathbf{q})$, with respect to the adopted sampling rate, revealing a somewhat involved structure with terms of the same order showing different dependence on this parameter, for example eqs. (15) and (17).

To contrast with the theoretical results, a commercial amplifier was characterized using four different types of waveforms and the coefficients of the model were extracted using an experimental setup with acquisition facilities. The model predictions were compared with the well-established memory polynomial behavioral model and performance is very similar, indicating the validity of the present procedure. Requiring a search algorithm for an abundant number or delays, the reference behavioral model exhibits somewhat better prediction of the output characteristics in the low power range. On the contrary, the introduced Volterra-based wideband behavioral method uses more delays without requiring a search process and outperforms the polynomial model in the range of powers where nonlinear effects are more significant.

An important requirement for a Volterra-based model is its ability to manage different types of signal. It has been revealed by observing the performance of the demonstrated model with input stimuli as diverse as a two-tone signal, a 3GPP W-CDMA signal and 16-QAM signal with rectangular and root-raised cosine pulses. The results were very satisfactory in all the cases. Because of space limitations, only the most relevant preliminary results have been presented. At the moment, the model is being tested with the experimental data in order to evaluate consistence at diverse measurement conditions and its ability to manage input signals with different bandwidths and power levels.

ACKNOWLEDGMENT

The authors wish to acknowledge the helpful assistance of T. J. Brazil and A. Zhu in the discussion of models complexity, and the useful comments received to improve the quality of the paper.

REFERENCES

[1] J. Kim and K. Konstantinou, "Digital predistortion of wideband signals based on power amplifier model with memory," *Electronics Letters*, vol. 37, no. 23, pp. 1417-1418, Nov. 2001.

[2] H. Ku and J. S. Kenney, "Behavioral Modeling of Nonlinear RF Power Amplifiers considering Memory Effects," *IEEE Trans. Microwave Theory and Tech.*, vol. 51, no. 12, pp. 2495–2504, Dec. 2003.

[3] A. Zhu and T. J. Brazil, "Behavioral Modeling of RF Power Amplifiers Based on Pruned Volterra Series," *IEEE Microw. Wireless Compon. Lett.*, vol. 14, no. 12, pp. 563–565, Dec. 2004.

[4] J. C. Pedro and S. A. Maas, "A Comparative Overview of Microwave and Wireless Power Amplifier Behavioral Approaches," *IEEE Trans. Microwave Theory and Tech.*, vol. 53, no. 4, pp. 1150–1163, Dec. 2005.

[5] J. Tsimbinos and K. V. Lever, "Computational complexity of Volterra based nonlinear compensators," *Electronics Letters*, vol. 32, no. 9, pp. 852-854, Apr. 1996.

[6] C. Crespo-Cadenas, J. Reina-Tosina, and M. J. Madero-Ayora, "Volterra series approach to behavioral modeling: application to an FET amplifier," Accepted to be presented at the *2006 IEEE Asia-Pacific Microwave Conference*, Yokohama, Japan, Dec. 2006.

[7] V. J. Mathews and G. L. Sicuranza, *Polynomial Signal Processing*, New York: Wiley, 2000.

[8] D. E. Dudgeon and R. M. Mersereau, *Multidimensional Digital Signal Processing*, New Jersey: Prentice Hall, 1984.

[9] C. H. Cheng and E. J. Powers, "Optimal Volterra Kernel Estimation Algorithms for a Nonlinear Communication System for PSK and QAM Inputs," *IEEE Trans. Signal Process.*, vol. 49, no. 1, pp. 147–163, Jan. 2001.

[10] J. J. Bussgang, L. Ehrman and J. W. Graham, "Analysis of Nonlinear Systems with Multiple Inputs," *Proceedings of the IEEE*, Vol. 62, No. 8, pp. 1088–1119, Aug. 1974.

[11] J. C. Pedro and N. Borges, *Intermodulation Distortion in Microwave and Wireless Circuits*, New York: Artech House, 2003.

[12] J. F. Sevic, K.L. Burger, and M. B. Steer, "A novel envelope-termination load-pull method for ACPR optimization of RF/Microwave power amplifiers," *1998 IEEE MTT-S Int. Microwave Symp. Dig.*, Baltimore, USA, June 1998, pp. 723–726.

[13] N. Borges and J. C. Pedro, "A Comprehensive Explanation of Distortion Sideband Asymmetries," *IEEE Trans. Microwave Theory and Tech.*, vol. 50, no. 9, pp. 2090–2101, Sep. 2002.

[14] J. Brinkhoff and A. E. Parker, "Effect of Baseband Impedance on FET Intermodulation," *IEEE Trans. Microwave Theory and Tech.*, vol. 51, no. 3, pp. 1045–1051, Mar. 2003.

[15] C. Crespo-Cadenas, J. Reina-Tosina, and M. J. Madero-Ayora, "Phase characterization of two-tone intermodulation distortion," presented at the *2005 IEEE MTT-S Int. Microwave Symp. Dig.*, Long Beach, USA, June 2005, pp. 1505-1508.

[16] C. Crespo-Cadenas, J. Reina-Tosina, and M. J. Madero-Ayora,, "IM3 and IM5 Phase Characterization and Analysis Based on a Simplified Newton Approach," *IEEE Trans. Microwave Theory and Tech.*, vol. 54, no. 1, pp. 321–328, Jan. 2006.

[17] J. Tsimbinos and K. V. Lever, "Input Nyquist Sampling Suffices to Identify and Compensate Nonlinear Systems," *IEEE Trans. Signal Process.*, vol. 46, no. 10, pp. 2833–2837, Oct. 1998.

Carlos Crespo-Cadenas was born in Madrid, Spain. He received the degree in Physics in 1973 and Doctor degree in 1995 from the Polytechnique University of Madrid. Since 1998 he has has been Associate Professor and currently he teaches lectures on Radio Communications in the Area of Signal Theory and Communications, University of Seville. His current interests are Nonlinear Analysis applied to Wireless Digital Communications and to Microwave Monolithic Integrated Circuits (MMIC).

Javier Reina-Tosina was born in Seville, Spain, in May 1973. He received the Telecommunication Engineering and Doctor degrees from the University of Seville, Seville, Spain, in 1996 and 2003, respectively. Since 1997 he has been with the Department of Signal Theory and Communications, University of Seville. His current research interests include MMIC technology, nonlinear analysis of active microwave devices and integration of information technologies in biomedicine.

María J. Madero-Ayora received the Telecommunication Engineering degree from the University of Seville, Seville, Spain, in 2002. Since 2003 she has been with the Department of Signal Theory and Communications, University of Seville, and is currently working toward the Doctor degree in Telecommunication Engineering. Her research interests lie in the area of nonlinear analysis of active microwave devices and measurement techniques for nonlinear communication systems.